Synthesis of indium oxide nanowires on quartz substrate for gas sensor

Abdulqader D. Faisal[1], Ali A. Aljubouri[1,*], and Wafaa Khalid Khalef[1]

[1] University of Technology, Department of Applied Sciences, Baghdad, Iraq
[*] Corresponding author. E-mail: 100372@uotechnology.edu.iq

Received: Nov. 17, 2019, Accepted: Apr. 07, 2020

In this paper, Indium oxide nanowires (In_2O_3 NWs) were successfully synthesized on quartz substrate pre-coated with gold nanoparticles (Au NPs) using chemical vapor deposition (CVD). The nanowires were characterized via x-ray diffraction (XRD), scanning electron microscope (SEM), Ultraviolet-Visible (UV-VIS) spectrophotometer. The sputtered of Au NPs on quartz were analyzed by atomic force microscopy (AFM). The structural, morphological, and optical properties were investigated. The XRD structure reviled a single crystal, with cubic crystal, with preferred orientation along (222). The SEM revealed nanowires growth. The obtained band gap value of 3.6 eV confirmed the formation of In_2O_3 nanostructures. Regarding to the characteristics of In_2O_3 NWs, it was fabricated as an ethanol gas sensor at 10-1500 ppm and an optimized temperature of 210 ^oC. The minimum ethanol gas response of Ra/Rg = 1.6 was obtained at a concentration of 10 ppm. The corresponding response and recovery time were achieved at the lowest concentration of 10 ppm is 10 s and 10 s respectively. So, the In_2O_3 NWs film synthesized via CVD can be considered as a good ethanol gas sensor device at low concentration. In_2O_3 NWs growth and gas sensing mechanism were also explained.

Keywords: Chemical vapor deposition (CVD); Gas sensor; In_2O_3 nanowires

http://dx.doi.org/10.6180/jase.202009_23(3).0010

1. Introduction

Air pollution is a major problem in today's world, a lot of people around the world breathe polluted air, without even thinking about the damage causes the lungs and the earth planet in general. Therefore, interest in the production of gas sensors has increased where; these sensors are characterized by their modest cost, high stability, nontoxicity, and their ability to detect a large number of toxic and volatile gases under various conditions [1, 2].

Metal oxide semiconductor (MOS) sensing devices including Fe_2O_3 [3], TiO_2 [4], ZnO [5], SnO_2 [6], CuO [7], and In_2O_3 [8], etc., have been extensively studied in the past few decades. Among these MOS, Indium oxide (In_2O_3) has got attention because of its unique physical and chemical properties, such as high electron affinity [9], high optical reflectance in the infrared region, high optical transmittance (greater than 90%) in the visible region of the electromagnetic radiation spectrum [10], and with a high electrical conductivity of the order of 10^4 $(\Omega.m)^{-1}$ [11].

In_2O_3 is extensively used in several applications such as optoelectronic devices [12], supercapacitors [13], lithium-ion batteries [14], solar cells [15], and gas sensors [16]. In_2O_3 is a promise n-type semiconductor with a body center cubic and hexagonal corundum structures and a wide direct band gap of 3.55-3.75 eV [17]. To improve the properties of gas sensors, it is very important to study the design of the shape and the size of the sediment. Thus, the synthesized In_2O_3 having different morphologies and sizes, such as nanobelts [18], nanosheets [[19], nanotubes [20], nanowires [21], nanorods [22], nanocubes [23], etc.. These morphologies are usually produced by many techniques such as pulsed laser deposition [24], hydrothermal [25], thermal evaporation [26], chemical vapor deposition (CVD) [27], etc. The CVD is a powerful technique to synthesize several nanostructure morphologies of In_2O_3 by changing the temperature as an example [28].

Many researchers investigated the formation of In_2O_3 nanowires at elevated temperatures (1300-1500^oC) [29, 30].

However, the synthesis of In_2O_3 nanowires at a temperature below 1000 °C is to be achieved, because it does not need costly equipment, low power consumption required and easy handling. The change in resistance of metal oxide sensors obtained when the surface of these sensors exposed to specific gas molecules [31].

In_2O_3 NWs has been previously used for gas sensor fabrication towards various reducing and oxidizing gases such as ethanol [32], acetone [33], H_2S [34], H_2 [35], NO_2 [36]. The growth and sensing mechanism of In_2O_3 NWs are also included within these articles.

In an n-type semiconductor, with oxidizing gases, the electrons will be withdrawn from the conduction band of the semiconducting material that is used as a gas sensor, resulting in a decrease in the conductivity of the metal oxide. On the other hand, in the presence of reducing gases, these gases react with oxygen molecules present at the surface of the semiconductor metal oxide resulting in an increase of the electrical conductivity of the sensing metal oxide [25].

Well known to improve the response and recovery times of In_2O_3 nanostructures sensors; their nanostructures size must be reduced or doping with convenient metal nanoparticles [35]. In addition, it is possible to obtain a material with a high sensitivity to gas sensing by controlling the morphology and structure of the material. These materials should exhibit a large surface to volume ratios [37].

In this work, In_2O_3 nanowires were synthesized via the CVD technique at 900 °C using flow N_2 gas. The fabricated ethanol gas sensor based on In_2O_3 NWs film on the quartz substrate at an optimal working temperature. The sensor confirms good sensitivity and low response and recovery time at 10 ppm ethanol gas.

2. Experimental

2.1. CVD preparation of In_2O_3 NWs

The indium oxide nanowires were synthesized by chemical vapor deposition (CVD) using 99.9% pure In_2O_3 powder as source material. The experimental diagram for In_2O_3 nanowires growth is shown in Fig. 1. The right side (outlet) of the quartz tube was connected to a water bubbler and the left side is connected to the nitrogen gas flow through a flow meter. A powder of 0.5 g was loaded on a small alumina boat (10 cm long) and positioned at the end of the miniature quartz tube of 2.5 cm diameter and 20 cm long, which is inserted in the center of the horizontal tube furnace keeping the alumina boat at the center of the furnace. A precleaned quartz substrate (1.5x1.5 cm^2) coated with 50 nm of gold films were positioned on 3 cm high of the powder. After loading the substrates, a constant flow of N_2 gas was fixed at 200 sccm. The growth temperature was raised to 900°C with a heating rate of 30°C/min. After maintaining the temperature at 900°C for 1h. The tube furnace was cooled down to room temperature naturally and a pale yellow material was found on the quartz substrates. The final product was characterized by AFM, XRD, SEM and UV-VIS spectrophotometer.

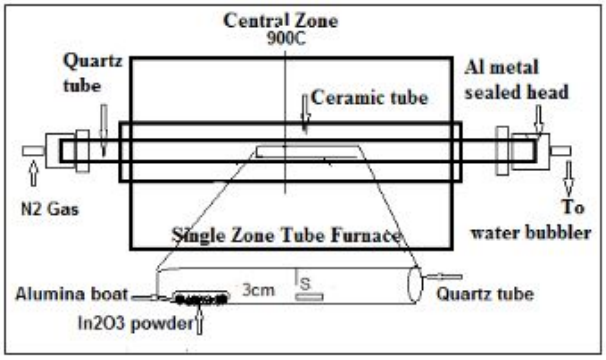

Fig. 1. CVD diagram for In_2O_3 nanowires grown on quartz substrates.

2.2. Characterization

The In_2O_3 nanostructures were characterized by atomic force microscope (AFM /SPM AA3000), X-ray diffraction (Shimadzu XRD-6000, X-ray diffractometer) using Cu Kα radiation (λ = 1.54056 Å) 2θ ranges from 20° to 80°. The morphology of the produced indium oxide nanostructure was investigated via scanning electron microscopy (SEM-Tescan Vega II- Cheek). Ultraviolet-Visible (UV–VIS) spectrophotometer (Shimadzu / UV-visible-2450 spectrophotometer) was used to calculate the bandgap energy of synthesized In_2O_3 NWs.

2.3. Gas sensor fabrication and measurements

The In_2O_3 NWs on the quartz substrate have been synthesized by chemical vapor deposition technique (CVD). These 1D nanostructures were fabricated for the ethanol gas sensor. The electrical contact was made on the top surface of the sensing materials by depositing two aluminum pads electrodes using physical vapor deposition (PVD). This sensor device fabrication is shown in Fig. 2a. The fabricated sensor device was mounted on the top of a homemade measurement stage as shown in Fig. 2b. This homemade stage is consisting of a miniature nickel-chromium heater placed at the backside of the quartz substrate. The operating temperature was measured by a k-type thermocouple fixed in the middle of the heater. The substrate temperature was controlled through an AC variable voltage to the heater coil to maintain at a desired operating temperature. Typically,

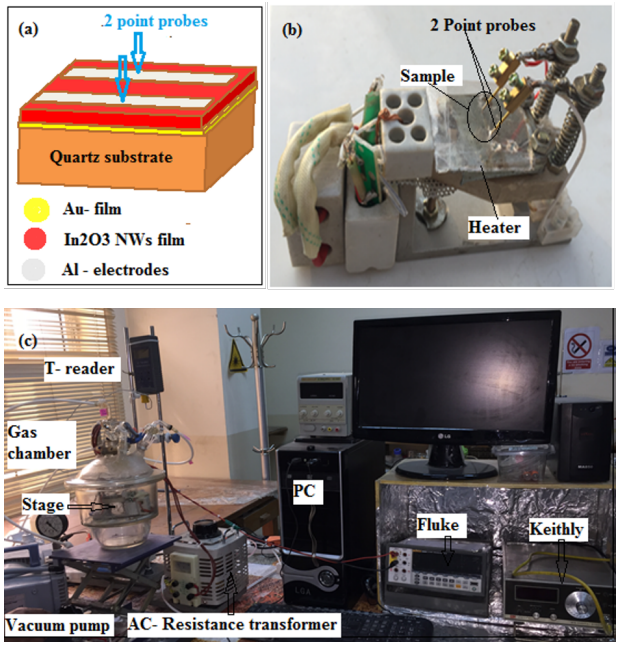

Fig. 2. Schematic diagram of (a) the fabricated sensor device, (b) Homemade measurement stage, (c) Gas sensor setup.

the miniaturized measurement stage was placed in a sealed chamber and the sensing experiments were conducted at the required conditions. Conductometric measurement through the two pointed electrodes was used to measure the resistance variation through the experiments. Figure 2c shows the homemade measurement stage inside the main gas chamber. The electrical measurements were conducted through wires connected to across feed-trough to the Keithley and Fluke electrometers. These are monitored by a computer through an interface. The gas sensor response was defined as $S = R_{air}/R_{gas}$, where R_{air} and R_{gas} are the resistances of the sensor in air and gas respectively.

3. Results and discussion

3.1. Structural properties

The gold nanoparticles as a catalyst material were sputtered on quartz substrate using DC sputtering technique with thicknesses of 50 nm. Before this deposition process, the chamber of the system was evacuated to 10^{-5} mbar. After that, the Au film removed from the system and it was annealed at 500°C in an argon atmosphere for 1h. Fig. 3 shows the 2D and 3D images of atomic force microscope (AFM) topography for a thin layer of Au nanoparticles. The grain size, average roughness (Sq), and the root mean square (RMS) roughness for the 50 nm of Au sputtered on quartz substrate are 95 nm, 0.57 nm, 0.68 nm, respectively.

The crystal structure of the synthesized In_2O_3 NWs on quartz substrate pre-coated with Au film is analyzed through the XRD pattern. Fig. 4 shows a typical XRD pattern of the grown In_2O_3 NWs obtained for 2θ scans between 20° and 80°. The diffraction peaks at 2θ = 30.64°, 35.49°, 51.05°, 60.73°, corresponding to the (222), (400), (440) and (622) planes of In_2O_3 NWs, which can be indexed to the body-centered cubic structure for In_2O_3 with a lattice constant of a=b=c= 10.117 Å according to the standard card of the crystallography open database (COD card no. 96-231-0010). The calculated value of the lattice constant in this work is 10.0858 Å, for the strongest diffraction peak at 2θ =30.6844°, which is corresponding to the (222) reflection plane. It is in a good agreement with this standard reference. Other diffraction peaks located at 2θ =38.3456°, 43.9744°, 64.9 and 77.488° are corresponding to the (111), (200), (220), and (311) planes of Au respectively, which are consistent with the standard card of the Crystallography Open Database (COD card no. 96-90-3039).

The crystallite size (D) for In_2O_3 NWs was calculated using Sherrer's formula:

$$D = 0.94\lambda/\beta cos\theta \quad (1)$$

Where λ is the wavelength of the x-ray Cu-Kα radiation (λ=1.5418 Å) source. β is the full width at half maximum of the diffraction peak corresponding to 2θ, θ is the Bragg diffraction angle. The calculated value of the crystallite size from Fig. 4 for the predominated diffraction peak at (222) reflection plane of In_2O_3 NWs was equal to 31.8 nm.

3.2. Morphological properties

Fig. 5 shows the SEM images of In_2O_3 NWs grown on quartz substrate coated with 50 nm of gold particles as a catalyst. A high density and homogenous distribution of vertically aligned nanowires with spherical gold particles sited at the NWs tips revealed by different magnifications of SEM images. The gold droplet size at the tips of the wires is larger than the diameters of the wires in Fig. 5. The AFM analysis confirmed these results.

3.2.1. *Growth mechanism of In_2O_3 NWs*

When the source material of In_2O_3 semiconductor sublimates at high temperature zone forming Sn metals vapor and oxygen molecules passing over a pre-coated layer of gold substrate as a catalyst. The gold particles forming a liquid droplet during the heating process. This droplet of Au will reach a saturation state when the source material vapors keep coming towards the substrate. During the supersaturating of Sn into Au droplet, a solute precipitates out from the droplet forming solid one-dimensional In_2O_3 nanowires. The gold spot can be localized at the top end

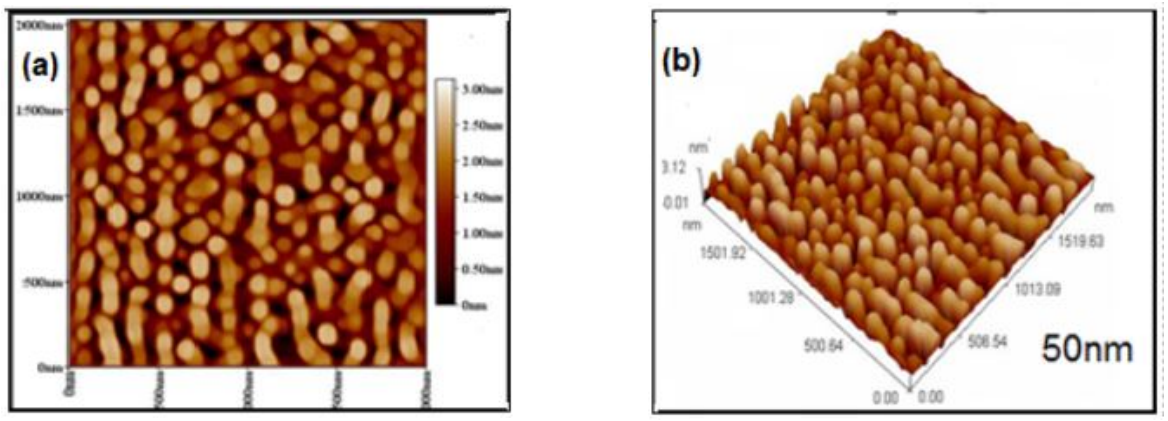

Fig. 3. 2D (a) and 3D (b) AFM images of Au NPs sputtered on quartz substrates with a thickness of 50 nm.

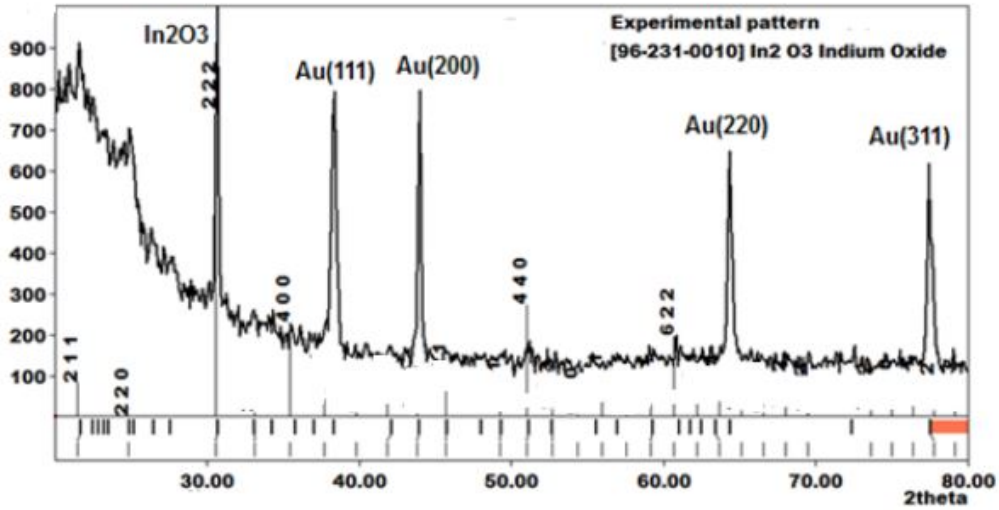

Fig. 4. XRD diffraction pattern of In_2O_3 grown on quartz, coated with an Au film of 50 nm.

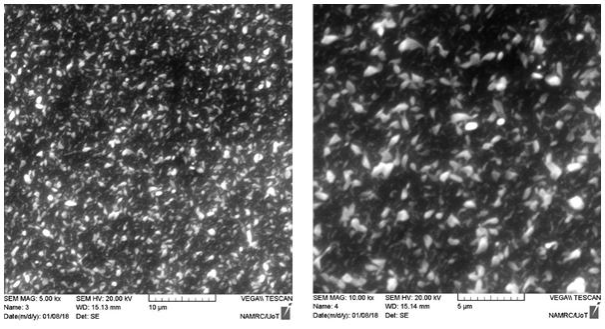

Fig. 5. SEM images for In_2O_3 NWs on quartz substrate coated with (50 nm) Au at different magnifications.

growing nanowires called tip growth process. This can be followed the vapor- liquid- solid (VLS) mechanism.

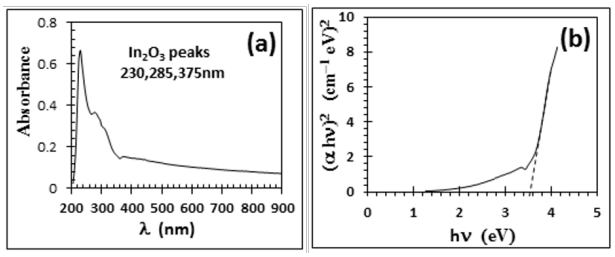

Fig. 6. (a) UV-Vis absorption spectra of In_2O_3 film deposited on quartz substrates. (b) E_g = 3.6 eV.

3.3. Optical properties

Fig. 6a shows a typical UV-Vis absorption spectrum of In_2O_3 NWs grown via CVD on quartz substrate pre-coated with gold catalysts. It exhibits an intense peak in the UV region centered at ~230 nm and other peaks with low intensity at 285 nm and 375 nm. The peak at ~230 nm is due to

interband transition of indium electrons from a deep level of the valence band (indicating the formation of indium oxide nonstructural, which was confirmed by SEM results), while peak below to 550 nm is due to interband transition of indium electrons from upper level of the valence band.

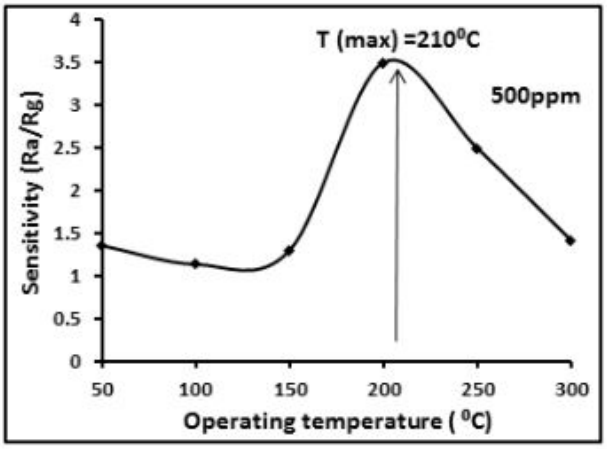

Fig. 7. Sensitivity versus temperature of synthesized In_2O_3 film via CVD technique.

The optical bandgap energy (E_g) of the as-synthesized nanoparticles are obtained from the UV-Vis spectra by using a well-known Tauc's relation [38], which is given by $\alpha h\vartheta = A\ (h\vartheta - E_g)^n$. Where $h\vartheta$ is the photon energy, A is a constant, which is a measure of crystalline order in the deposited films, and n = 0.5, 1.5, 2 or 3 for allowed-direct, forbidden-direct, allowed-indirect, and forbidden-indirect electronic transitions, respectively. In this case, the bandgap energy (E_g) has been estimated by assuming an allowed direct electronic transition between the highest occupied state of the valence band and the lowest unoccupied state of the conduction band. Fig. 6b shows the dependence of the absorption coefficients $(\alpha h\vartheta)^2$ on photon energy ($h\vartheta$) for the prepared films. The energy bandgap (Eg), of the film, was obtained by extrapolating the linear portion (part) of the plot of $(\alpha h\vartheta)^2$ against photon energy ($h\vartheta$) to $(\alpha h\vartheta)^2 = 0$. The bandgap of as-deposited In_2O_3 NWs is 3.6 eV.

The bandgap of the synthesized In_2O_3 is lesser than the bandgap of bulk In_2O_3 (3.75 eV), which is due to the occurrence of a weak quantum confinement effect [39]. In this work, the obtained value of the energy gap is closed to the presented values in article [40].

3.4. Gas sensor properties

The operating temperature of the sensor was found when exposing the sensor to 500 ppm of ethanol at different operating temperatures. Fig. 7 shows the responses of the sensor increased by increasing the operating temperature.

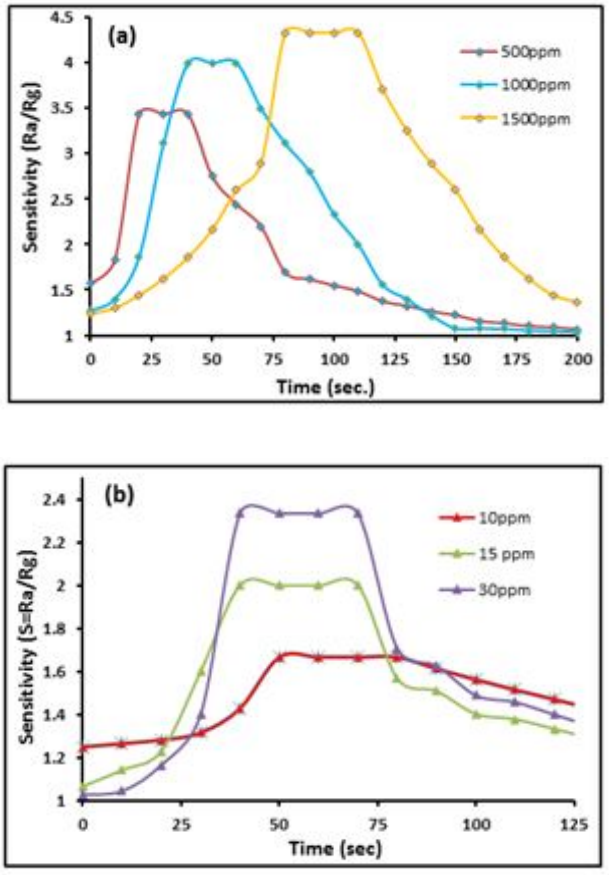

Fig. 8. Typical gas sensing responses (R_a/R_g) of the In_2O_3 sensor at high and low ethanol concentrations (a and b respectively) and at the operating temperature of 210 ºC.

The maximum response value around 3.5 was observed at the operating temperature of 210 °C. This high response of In_2O_3 NWs film prepared by a CVD technique is attributed to a high surface to volume ratio.

A typical gas response versus time at high and low ethanol concentrations is demonstrated as shown in Figs. 8a and b, respectively. In both sets of curves, the gas response starts to increase after the ethanol gas injected into the reaction chamber and reaches a saturation level, and then decreased when the sample is exposed to the air. They have an identical behavior in a sensing response. It was found that the gas response is equal to Ra/Rg = 3.5 at a moderate ethanol concentration of 500 ppm and at an optimized temperature of 210 ºC as shown in Fig. 8a. This is a higher response than the value reported for indium oxide thin film at 400 ppm [40]. The minimum ethanol gas response of Ra/Rg = 1.6 was also obtained at a concentration of 10 ppm and at an optimized temperature of 210 ºC as shown in Fig. 8b. This is also higher than the

reported value for individual In_2O_3 NWs prepared by the carbothermal reduction method [41].

Fig. 9 demonstrates the sensitivity variation versus the ethanol concentrations in the range of 10-1500 ppm at an optimized operating temperature of 210 °C. The inset of this figure shows a magnified curve for the low ethanol concentrations. Both curves at high and low ethanol concentrations having similar behavior. Therefore, it could be confirmed the principle of high sensitivity at a high concentration of gas and vice versa. Thus, this sensor material is considered as a promising candidate for ethanol gas sensing.

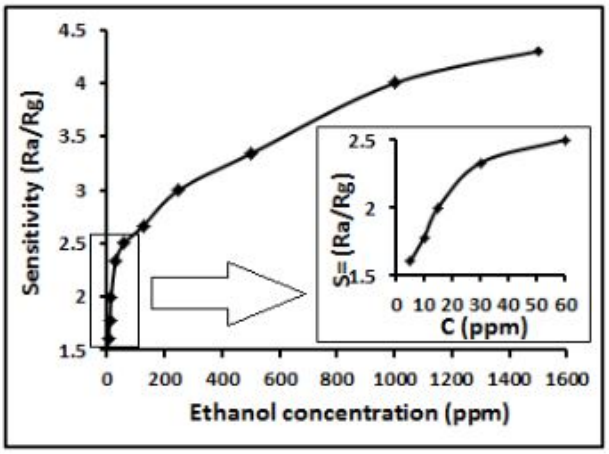

Fig. 9. Sensitivity versus different ethanol concentrations of In_2O_3 film operating at an optimized temperature of 210 °C. (Inset represents the low concentration data).

The response and recovery time are important parameters for evaluating the sensor. The response time (t_{resp}) is defined, as the time required achieving 90% of the total resistance change when the ethanol gas is introduced into the chamber. The recovery time, (t_{recov}), is the time that required reaching 90% of the total resistance change when the target gas is turned off, and the air is re-introduced into the chamber. Fig. 10 represents the response and recovery time characteristics versus ethanol gas concentrations. The response and recovery time curves were increased slowly as the ethanol gas concentrations increased as shown in Fig. 10a. The response and recovery time values at high ethanol concentrations of 500-1500 ppm are 15-30 s and 30-80 s, respectively. Fig. 10b shows low ethanol concentrations of 10-30 ppm given lower response and recovery time values of 10-15 s and 10-30 s, respectively. Moreover, the minimum response and recovery time values at the lowest concentration of 10 ppm are 10 s for both of them as shown in Fig. 10b. This is considered as ultimate parameters for the In_2O_3 NWs film synthesized via CVD.

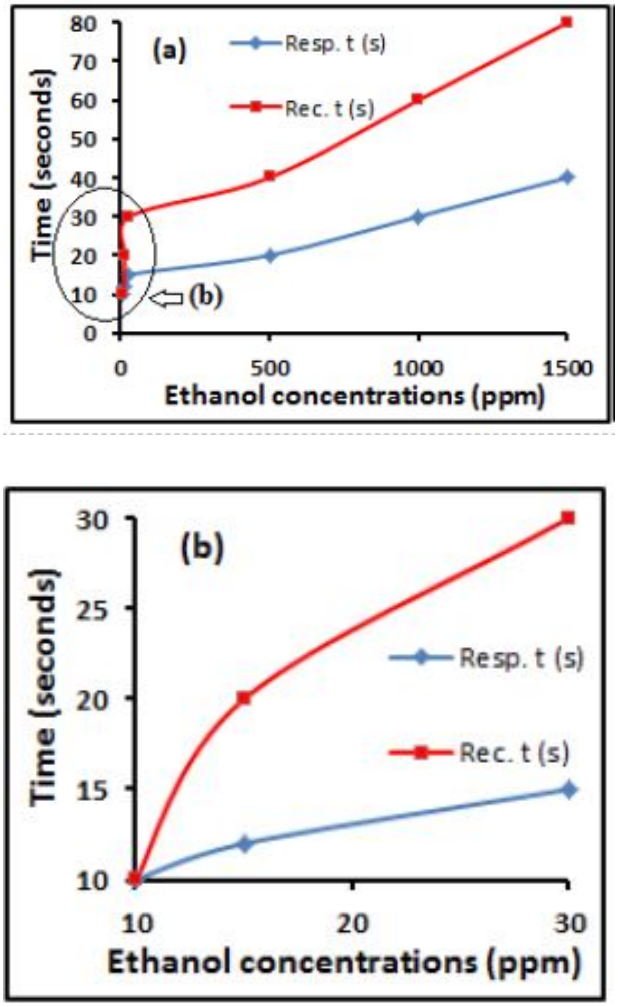

Fig. 10. Response and recovery time versus ethanol gas concentrations of In_2O_3 film operating at an optimized temperature of 210 °C. (Inset represents the low concentration data).

4. Conclusion

In a summary conclusion, the In_2O_3 NWs were synthesized on quartz substrates coated with a gold film of 50 nm thickness, via CVD technique using In_2O_3 powder, which was evaporated at 900 °C for 1h with the N_2 gas flow only. The XRD pattern was confirmed the crystalline structures of a well oriented single crystal along direction of [222] with small gold. The SEM images reveal the formation of In_2O_3 nanowires. The large droplet of gold at the end of the wires. The results of gas sensor's performance for ethanol vapor provide high sensitivity at an optimized working temperature. Based on the response towards ethanol gas for different concentrations has been studied and the minimum response was found at 10 ppm with fast response

and recovery time of 10 s and 10 s, respectively. In our investigation, high sensitivity of fast response and recovery time are found to be at an operating temperature of 210 °C. These facts confirm that In_2O_3 NWs film produced via CVD technique for 500 ppm ethanol is an effective method for ethanol gas sensing applications at a concentration range from 10 ppm – 1500 ppm.

References

[1] Antonio Tricoli, Marco Righettoni, and Alexandra Teleki. Semiconductor Sensors Semiconductor Gas Sensors : Dry Synthesis and Application Angewandte. *Wiley Online Library*, pages 7632–7659, 2010.

[2] Niranjan S. Ramgir, Yang Yang, and Margit Zacharias. Nanowire-based sensors, aug 2010.

[3] Qianqiu Tang, Wenqiang Wang, and Gengchao Wang. The perfect matching between the low-cost Fe2O3 nanowire anode and the NiO nanoflake cathode significantly enhances the energy density of asymmetric supercapacitors. *Journal of Materials Chemistry A*, 3(12):6662–6670, 2015.

[4] Prabhakar Rai, Yun Su Kim, Hyeon Min Song, Min Kyung Song, and Yeon Tae Yu. The role of gold catalyst on the sensing behavior of ZnO nanorods for CO and NO 2 gases. *Sensors and Actuators, B: Chemical*, 165(1):133–142, 2012.

[5] P. M. Perillo and D. F. Rodríguez. The gas sensing properties at room temperature of TiO2 nanotubes by anodization. *Sensors and Actuators, B: Chemical*, 171-172:639–643, 2012.

[6] Abhijit A. Yadav. SnO2 thin film electrodes deposited by spray pyrolysis for electrochemical supercapacitor applications. *Journal of Materials Science: Materials in Electronics*, 27(2):1866–1872, feb 2016.

[7] Ali A. Aljubouri, Abdulqader D. Faisal, and Wafaa K. Khalef. Fabrication of temperature sensor based on copper oxide nanowires grown on titanium coated glass substrate. *Materials Science- Poland*, 36(3):460–468, 2018.

[8] Bingxin Xiao, Fei Wang, Chengbo Zhai, Pan Wang, Chuanhai Xiao, and Mingzhe Zhang. Facile synthesis of In2O3 nanoparticles for sensing properties at low detection temperature. *Sensors and Actuators, B: Chemical*, 235:251–257, 2016.

[9] Maryam Amirhoseiny, Zainuriah Hassan, and Ng Shashiong. Synthesis of nanocrystalline In2O3 on different Si substrates at wet oxidation environment. *Optik*, 124(17):2679–2681, 2013.

[10] Xiumei Xu, Dawei Wang, Jing Liu, Peng Sun, Yue Guan, Heng Zhang, Yanfeng Sun, Fengmin Liu, Xishuang Liang, Yuan Gao, and Geyu Lu. Template-free synthesis of novel In2O3 nanostructures and their application to gas sensors. *Sensors and Actuators, B: Chemical*, 185:32–38, 2013.

[11] K. P. Sibin, Niharika Swain, Prasanta Chowdhury, Arjun Dey, N. Sridhara, H. D. Shashikala, Anand Kumar Sharma, and Harish C. Barshilia. Optical and electrical properties of ITO thin films sputtered on flexible FEP substrate as passive thermal control system for space applications. *Solar Energy Materials and Solar Cells*, 145:314–322, 2016.

[12] Bishnu Prasad Bastakoti, Hamid Oveisi, Chi Chang Hu, Kevin C.W. Wu, Norihiro Suzuki, Kimiko Takai, Yuichiro Kamachi, Masataka Imura, and Yusuke Yamauchi. Mesoporous carbon incorporated with In2O3 nanoparticles as high-performance supercapacitors. *European Journal of Inorganic Chemistry*, (7):1109–1112, mar 2013.

[13] M Osiak, W Khunsin, E Armstrong, T Kennedy, C. M.Sotomayor Torres, K M Ryan, and C. O'Dwyer. Epitaxial growth of visible to infra-red transparent conducting In 2O3 nanodot dispersions and reversible charge storage as a Li-ion battery anode. *Nanotechnology*, 24(6):65401–65411, 2013.

[14] Dong Ju Kim and Han Ki Kim. Optimization of titanium-doped indium oxide anodes for heterojunction organic solar cells. *Physica Status Solidi (A) Applications and Materials Science*, 214(2), feb 2017.

[15] Zhao Qiang Zheng, Lian Feng Zhu, and Bing Wang. In2O3 Nanotower Hydrogen Gas Sensors Based on Both Schottky Junction and Thermoelectronic Emission. *Nanoscale Research Letters*, 10(1), dec 2015.

[16] Pei Li, Huiqing Fan, Yu Cai, and Mengmeng Xu. Zn-doped In2O3 hollow spheres: Mild solution reaction synthesis and enhanced Cl2 sensing performance. *CrystEngComm*, 16(13):2715–2722, apr 2014.

[17] Su Zhang, Peng Song, Zhongxi Yang, and Qi Wang. Facile hydrothermal synthesis of mesoporous In2O3 nanoparticles with superior formaldehyde-sensing properties. *Physica E: Low-Dimensional Systems and Nanostructures*, 97:38–44, 2018.

[18] Chang Sup Moon, Hae Ryong Kim, Graeme Auchterlonie, John Drennan, and Jong Heun Lee. Highly sensitive and fast responding CO sensor using SnO2 nanosheets. *Sensors and Actuators, B: Chemical*, 131(2):556–564, 2008.

[19] Changhui Zhao, Baoyu Huang, Erqing Xie, Jinyuan Zhou, and Zhenxing Zhang. Improving gas-sensing properties of electrospun In2O3 nanotubes by Mg acceptor doping. *Sensors and Actuators, B: Chemical*, 207(Part A):313–320, 2015.

[20] Yu Cian Wang, Chih Yao Chen, Cheng Wen Kuo, Ta Ming Kuan, Cheng Yeh Yu, and I. Chen Chen. Low-temperature grown indium oxide nanowire-based antireflection coatings for multi-crystalline silicon solar cells. *Physica Status Solidi (A) Applications and Materials Science*, 213(8):2259–2263, aug 2016.

[21] Zhi Xuan Cheng, Xiang Bing Dong, Qing Yi Pan, Jian cheng Zhang, and Xiao Wen Dong. Preparation and characterization of In2O3 nanorods. *Materials Letters*, 60(25-26):3137–3140, 2006.

[22] Jun Yang, Chunxia Li, Zewei Quan, Deyan Kong, Xiaoming Zhang, Piaoping Yang, and Jun Lin. One-step aqueous solvothermal synthesis of in 2O 3 nanocrystals. *Crystal Growth and Design*, 8(2):695–699, feb 2008.

[23] Zaiyin Huang, Chunfang Chai, Xuecai Tan, Jian Wu, Aiqun Yuan, and Zeguang Zhou. Photoluminescence properties of the In2O3 octahedrons synthesized by carbothermal reduction method. *Materials Letters*, 61(29):5137–5140, 2007.

[24] Po Chiang Chen, Guozhen Shen, Saowalak Sukcharoenchoke, and Chongwu Zhou. Flexible and transparent supercapacitor based on In2 O 3 nanowire/carbon nanotube heterogeneous films. *Applied Physics Letters*, 94(4), 2009.

[25] Sergio Roso, Toni Vilic, Atsushi Urakawa, and Eduard Llobet. Gas Sensing Properties of In2O3 Cubes Prepared by a Hydrothermal Method. In *Procedia Engineering*, volume 168, pages 247–250, 2016.

[26] Liu Jian, Huang Shihua, and He Lö. Metal-catalyzed growth of In2O3 nanotowers using thermal evaporation and oxidation method. *Journal of Semiconductors*, 36(12), 2015.

[27] Fatma Nur Tuzluca, Yasar Ozkan Yesilbag, Tuba Akkus, and Mehmet Ertugrul. Effects of graphite on the synthesis of 1-D single crystal In2O3 nanostructures at high temperature. *Materials Science in Semiconductor Processing*, 66:62–68, 2017.

[28] Ahsanulhaq Qurashi, E. M. El-Maghraby, Toshinari Yamazaki, and Toshio Kikuta. Catalyst supported growth of In2O3 nanostructures and their hydrogen gas sensing properties. *Sensors and Actuators, B: Chemical*, 147(1):48–54, 2010.

[29] Zheng Wei Pan, Zu Rong Dai, and Zhong Lin Wang. Nanobelts of semiconducting oxides. *Science*, 291(5510):1947–1949, 2001.

[30] Y. Li, Y. Bando, and D. Golberg. Single-Crystalline In2O3 Nanotubes Filled with In. *Advanced Materials*, 15(78):581–585, apr 2003.

[31] N Barsan, D Koziej, U Weimar Sensors Chemical, Actuators B:, and Undefined 2007. Metal oxide-based gas sensor research: How to? *Sensors and Actuators, B: Chemical*, 121(1):18–35, 2007.

[32] Guillem Domènech-Gil, Jordi Samà, Paolo Pellegrino, Sven Barth, Isabel Gràcia, Carles Cané, and Albert Romano-Rodriguez. Gas nanosensors based on individual indium oxide nanostructures. In *Procedia Engineering*, volume 120, pages 795–798, 2015.

[33] A Vomiero, S Bianchi, E Comini, G Faglia, M. Ferroni, N. Poli, and G. Sberveglieri. In2O3 nanowires for gas sensors: morphology and sensing characterisation. *Thin Solid Films*, 515(23):8356–8359, 2007.

[34] Zhongming Zeng, Kai Wang, Zengxing Zhang, Jiajun Chen, and Weilie Zhou. The detection of H2S at room temperature by using individual indium oxide nanowire transistors. *Nanotechnology*, 20(4), 2009.

[35] Ahsanulhaq Qurashi, E. M. El-Maghraby, Toshinari Yamazaki, Yanbai Shen, and Toshio Kikuta. A generic approach for controlled synthesis of In2O3 nanostructures for gas sensing applications, 2009.

[36] Pengcheng Xu, Zhixuan Cheng, Qingyi Pan, Jiaqiang Xu, Qun Xiang, Weijun Yu, and Yuliang Chu. High aspect ratio In2O3 nanowires: Synthesis, mechanism and NO2 gas-sensing properties. *Sensors and Actuators, B: Chemical*, 130(2):802–808, 2008.

[37] T Wagner, T Sauerwald, C. D. Kohl, T. Waitz, C. Weidmann, and M. Tiemann. Gas sensor based on ordered mesoporous In2O3. *Thin Solid Films*, 517(22):6170–6175, 2009.

[38] E. F. Keskenler, G Turgut, and S. Doğan. Investigation of structural and optical properties of ZnO films co-doped with fluorine and indium. *Superlattices and Microstructures*, 52(1):107–115, 2012.

[39] Chang Hoon Lee, Minsik Kim, Taekhoon Kim, Ansoon Kim, Jungsun Paek, Ju Wook Lee, Sung Yool Choi, Kyuwon Kim, Jong Bong Park, and Kwangyeol Lee. Ambient pressure syntheses of size-controlled corundum-type In2O3 nanocubes. *Journal of the American Chemical Society*, 128(29):9326–9327, jul 2006.

[40] K. K. Makhija, Arabinda Ray, R. M. Patel, U. B. Trivedi, and H. N. Kapse. Indium oxide thin film based ammonia gas and ethanol vapour sensor. *Bulletin of Materials Science*, 28(1):9–17, 2005.

[41] Guillem Domènech-Gil, Sven Barth, Jordi Samà, Paolo Pellegrino, Isabel Gràcia, Carles Cané, and Albert Romano-Rodriguez. Gas sensors based on individual indium oxide nanowire. *Sensors and Actuators, B: Chemical*, 238:447–454, 2017.